ACS SENSORS

Article

pubs.acs.org/acssensors

Modulating Selectivity in Nanogap Sensors

Hamid Reza Zafarani,[†] Klaus Mathwig,[‡] Serge G. Lemay,[§] Ernst J. R. Sudhölter,[†] and Liza Rassaei*[,†]

[†]Laboratory of Organic Materials and Interfaces, Department of Chemical Engineering, Delft University of Technology, Van der Maasweg 9, 2629 HZ Delft, The Netherlands

[‡]Pharmaceutical Analysis, Groningen Research Institute of Pharmacy, University of Groningen, P.O. Box 196, 9700 AD Groningen, The Netherlands

[§]MESA+ Institute for Nanotechnology, University of Twente, P.O. Box 217, 7500 AE Enschede, The Netherlands

Supporting Information

ABSTRACT: Interference or crosstalk of coexisting redox species results in overlapping of electrochemical signals, and it is a major hurdle in sensor development. In nanogap sensors, redox cycling between two independently biased working electrodes results in an amplified electrochemical signal and an enhanced sensitivity. Here, we report new strategies for selective sensing of three different redox species in a nanogap sensor of a 2 fL volume. Our approach relies on modulating the electrode potentials to define specific potential windows between the two working electrodes; consequently, specific detection of each redox species is achieved. Finite element modeling is employed to simulate the electrochemical processes in the nanogap sensor, and the results are in good agreement with those of experiments.

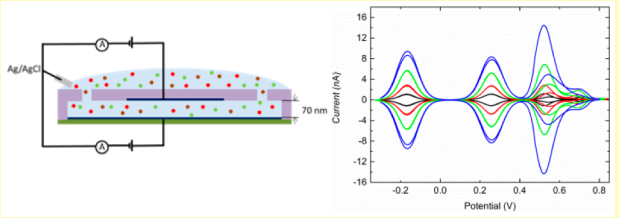

KEYWORDS: *redox cycling, nanogap sensor, nanoelectrochemistry, nanofluidics, selectivity*

Selective detection of redox species is important in various fields such as pharmacy,[1−3] pathology,[4,5] health,[6−8] and environmental monitoring.[9,10] Interference or crosstalk of coexisting compounds leads to the overlap of electrochemical responses and is one major drawback of these techniques; frequently encountered, it impedes simultaneous detection of species and limits the selectivity of electrochemical sensors.[11,12] Thus, many research efforts have been devoted to overcoming this hurdle, for example, by electrochemically pretreating electrodes;[13] using different electrode materials;[14] modifying electrodes with organic compounds,[15,16] polymers,[17,18] or nanoparticles;[10,19,20] adding complexing agents to the solution;[21] or by using a combination of these methods.[22,23]

Sensing redox species using dual electrodes benefits from amplified electrochemical signals and enhanced sensitivity while the contribution from the background current is minimized.[24,25] In such systems, one electrode is biased at the reduction potential and the other at the oxidation potential. Here, the redox-active species undergo successive oxidation and reduction reactions as they travel by diffusion between these closely spaced electrodes. Hence, the Faradaic current is amplified and the sensitivity is enhanced. Interdigitated electrodes (IDE)—as one of the well-known classes of dual electrode systems—have been widely used in different studies.[26−28] IDEs consist of a pair of comb-shaped opposing electrodes with interlocking teeth in which each set of electrodes can be independently biased.

A newer type of dual electrode systems is the electrochemical nanofluidic devices which consist of two planar parallel electrodes closely spaced (<100 nm) from each other in a nanofluidic channel.[29−31] The interferences in these nanogap devices[29,32,33] have mainly been eliminated by biasing one electrode at the potential that consumes the interference while the other electrode is swept to quantify the target analyte.[34,35] The nanogap is depleted from interfering irreversible redox species and the signal for the analyte is insensitive to the interfering species. However, this method only eliminates the response from interfering irreversible redox species. Therefore, a more versatile technique is required to overcome the interferences from reversible redox species in these nanogap sensors.

In the present work, we introduce a new method to selectively detect three reversible redox species in the nanogap sensors. The method relies on modulating the potentials of both electrodes in a way that each species is separately detected. We implement this method for the simultaneous detection of these three species in three different ways unique to dual-electrode sensors: (a) by cyclic voltammetry and varying the fixed potential of the second working electrode; (b) by differential cyclic voltammetry (DCV);[36,37] and (c) by potential step chronoamperometry. Finite element analysis (COMSOL Multiphysics) is employed to model the electrochemical processes in the nanogap sensor and compare with those of experiments.

Received: September 2, 2016
Accepted: October 26, 2016
Published: October 26, 2016

DOI: 10.1021/acssensors.6b00556
ACS Sens. 2016, 1, 1439−1444

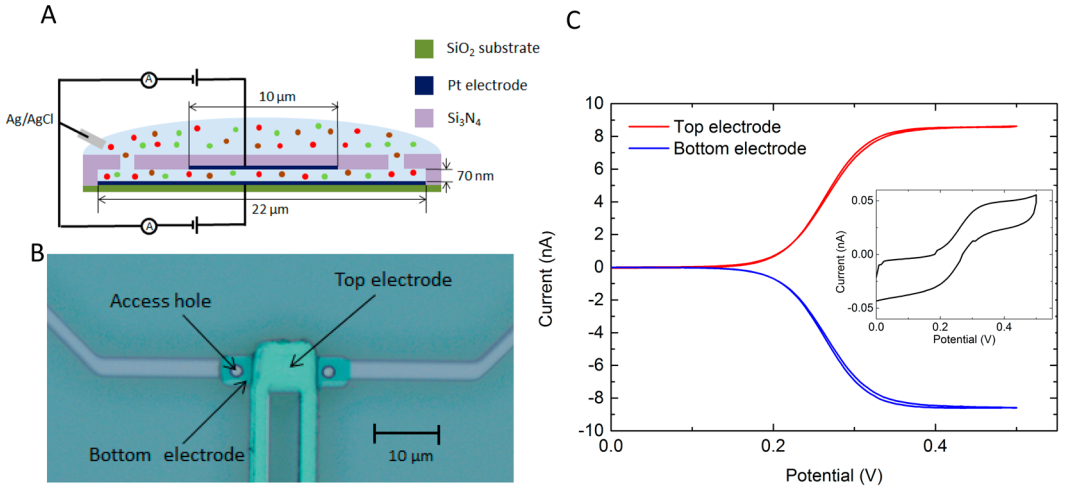

Figure 1. (A) Schematic view of the nanogap device. (B) Optical micrograph of a nanogap sensor (top view). (C) Cyclic voltammogram of 0.33 mM $Fc(MeOH)_2$ in 1 M KCl solution. The top electrode was swept between 0 and 0.5 V (vs Ag/AgCl) at a 10 mV s^{-1} scan rate while the bottom electrode was kept at 0 V. The inset figure shows a cyclic voltammogram in single mode; the top electrode was swept vs Ag/AgCl while the bottom electrode was kept floating.

EXPERIMENTAL SECTION

Chemicals. 1,1′-Ferrocene dimethanol, $Fc(MeOH)_2$, hexaammineruthenium(III) chloride, $Ru(NH_3)_6Cl_3$, and potassium iodide, KI, as electroactive model compounds; potassium chloride, KCl, and standard chromium etchant were purchased from Sigma-Aldrich. All solutions were freshly prepared in Milli-Q water with 1 M KCl as supporting electrolyte and the experiments were carried out at room temperature.

Nanogap Device Fabrication. Nanogap devices were fabricated on a silicon wafer covered with 500 nm thermally grown SiO_2, employing several lithography steps and evaporation as previously reported.[30] In brief, a nanogap device consisted of a platinum bottom electrode of a 22 μm by 3 μm surface area and a top electrode of 10 μm by 9 μm. A 70-nm-thick sacrificial chromium layer between these two electrodes defined the volume of the nanochannel. The whole device was covered in a 500 nm silicon oxide/silicon nitride passivation layer in which access holes to the chromium layer were dry etched. Before measurements, the chromium layer was etched away using chromium etchant leaving behind a nanogap sensor. A schematic and optical micrograph of a nanogap device are presented in Figure 1A and B.

Electrochemical Measurements. Electrochemical experiments were carried out using a Keithley 4200 parameter analyzer with two source measurement units (SMUs). The SMUs were used as voltage source and current detection elements to separately bias both electrodes and measure faradic currents. A commercial Ag/AgCl electrode (BASi Inc.) was used as a reference, positioned in a reservoir on top of the nanogap device.

Numerical Methods. Two-dimensional finite element analysis was carried out using COMSOL Multiphysics to simulate the electrochemical processes in the nanochannel with conditions similar to those for the experimental measurements.[38] Assuming a highly concentrated supporting electrolyte and an unstirred solution, diffusion was considered as the only mass transport mechanism in the nanogap sensor as described by Fick's second law:

$$\frac{\partial C_j}{\partial t} = D_j \nabla^2 C_j \tag{1}$$

Here, C_j and D_j are the concentration and diffusion coefficient of a redox species j, respectively. The currents are defined based on Butler–Volmer kinetics:[39]

$$i = F[c_O k_f - c_R k_b] \tag{2}$$

$$k_f = k_0 \exp\left[\frac{-\alpha F(E - E_h)}{RT}\right] \tag{3}$$

$$k_b = k_0 \exp\left[\frac{(1 - \alpha) F(E - E_h)}{RT}\right] \tag{4}$$

Here, i is the current, k_0 is the mass transfer coefficient, α the charge transfer coefficient, F the Faraday constant, E the electrode potential, E_h the redox potential of the redox couple, k_f and k_b are the forward (reduction) and backward (oxidation) rate constants of a redox reaction, R is the gas constant, T the temperature, c_O and c_R are the concentration of oxidized and reduced species, respectively.

Table 1 lists constants used in the simulations, including diffusion coefficients D and redox potentials (vs Ag/AgCl), E_h, for the $Fc(MeOH)_2$, KI, and $Ru(NH_3)_6Cl_3$ redox couples. An identical rate constant k_0 and transfer coefficients α were assumed for all species.

Table 1. Parameters Used in the Simulation Processes[30,37,40−42]

$D_{Fc(MeOH)_2}$	6.7×10^{-10} m^2/s	α	0.49
D_{I^-}	2.05×10^{-9} m^2/s	F	96485.34 C/mol
$D_{Ru(NH_3)_6^{3+}}$	7.5×10^{-10} m^2/s	R	8.31 J/K
$E_{h,Fc(MeOH)_2}$	0.26 V vs Ag/AgCl	T	298 K
E_{h,I^-}	0.54 V vs Ag/AgCl	k_0	0.06 m/s
$E_{h,Ru(NH_3)_6^{3+}}$	−0.16 V vs Ag/AgCl		

RESULTS AND DISCUSSION

Amplification Factor. Figure 1C shows the cyclic voltammograms obtained from the redox cycling of 0.33 mM 1,1′-ferrocene dimethanol in 1 M potassium chloride in the nanogap sensor. The inset in this figure presents the cyclic voltammogram obtained in single mode: only the top electrode was swept and the bottom electrode was left floating. Identical measurements were carried out for $Ru(NH_3)_6Cl_3$ and potassium iodide (see Figure S1 in the Supporting Information). Comparing the limiting currents in these two modes, I_{dual}/I_{single}, leads to an amplification factor of 170 corresponding to a gap height of 74 nm according to[33]

DOI: 10.1021/acssensors.6b00556
ACS Sens. 2016, 1, 1439−1444

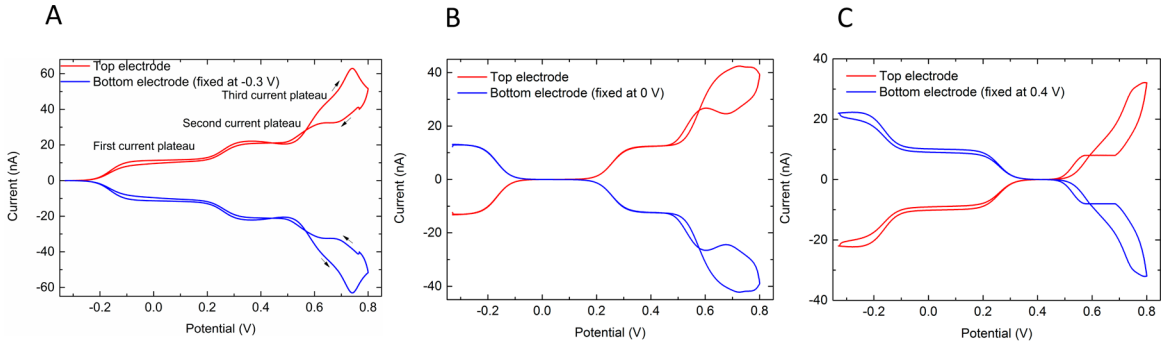

Figure 2. Cyclic voltammetry of a mixture of 0.33 mM $Ru(NH_3)_6^{3+}$, 0.33 mM $Fc(MeOH)_2$, and 0.33 mM I^- in a 1 M KCl solution. The top electrode is swept between −0.33 and 0.8 V at a scan rate of 10 mV s^{-1}, and the bottom electrode potential is fixed at (A) −0.3 V, (B) 0 V, and (C) 0.4 V. Arrows (A) indicate the scan direction.

$$I = \frac{nFADC}{z} \tag{5}$$

where I is limiting Faradaic current for two planar electrodes in close distance, n is the number of electrons transferred in the redox reaction, A is the overlapping area between the two electrodes, and z is the distance between the electrodes, i.e., the nanochannel height.

Tuning Electrodes' Potentials for Separate Detection of Each Species. Conventional electrochemical measurements suffer from poor selectivity, because, in a mixture of various reduced (or oxidized) electroactive species having different standard redox potentials, all species are simultaneously oxidized (or reduced) when a high (or low) enough electrode potential is applied. The interferences caused this way complicate the interpretation of the results as the electro-oxidation (or electro-reduction) current for the redox species with the highest oxidation (or lowest reduction) potential is superimposed by the signals from the other redox species.

Nanogap sensors not only allow amplifying the electrochemical signals of redox species, but also open up the possibility to prevent such interferences. The two working electrodes in the nanogap sensor are independently biased and, thus, they enable selective electrochemical reactions of specific redox couples. Selective detection is achieved by defining the potentials of the two electrodes in a way in which only the target species undergoes redox cycling. Simultaneously, interfering species are also reduced or oxidized but they do not undergo redox cycling, and therefore, the signal of these species is not amplified.

Figure 2 shows cyclic voltammograms for a mixture of 0.33 mM $Fc(MeOH)_2$, 0.33 mM $Ru(NH_3)_6^{3+}$ and 0.33 mM I^- as three redox active species in 1 M KCl solution. Varying the bottom electrode potential to certain fixed potentials leads to a separate detection of these species in specific potential ranges. Here, the top electrode is swept between −0.33 and 0.8 V (vs Ag/AgCl) while the potential of the bottom electrode is kept at −0.3, 0, and 0.4 V, respectively.

In Figure 2A, the potential of the bottom electrode is set at −0.3 V. As presented, the potential of the top electrode is scanned from −0.3 V, and the first current plateau corresponds to redox cycling of $Ru(NH_3)_6^{3+/2+}$ ions (E_h = −0.16 V) without any interference from the other two species; the second current plateau relates to the combined redox cycling of $Fc(MeOH)_2^{0/+1}$ (E_h = 0.26 V) and $Ru(NH_3)_6^{3+/2+}$ ions. The third current plateau associates with the redox cycling of I^- (E_h = 0.54 V) and the previous two species. The redox reactions of the species are as follows:

$$Fc(MeOH)_2 \rightleftarrows Fc(MeOH)_2^+ + e^- \tag{6}$$

$$Ru(NH_3)_6^{3+} + e^- \rightleftarrows Ru(NH_3)_6^{2+} \tag{7}$$

$$I^- \rightleftarrows 1/2I_2 + e^- \tag{8}$$

Once the potential of the bottom electrode is changed to 0 V (see Figure 2B), the interference and the contribution of $Ru(NH_3)_6^{3+/2+}$ ions on redox cycling of $Fc(MeOH)_2^{0/+1}$ and I^- disappears. As presented in this figure, here, redox cycling of $Ru(NH_3)_6^{3+/2+}$ occurs in the potential window of −0.3 to −0.16 V. For potentials above −0.16 V, $Ru(NH_3)_6^{3+/2+}$ ions exist in the oxidized form and cannot undergo redox cycling anymore. Hence, their contribution to the redox cycling currents of $Fc(MeOH)_2^{0/+1}$ and I^- is eliminated. This allows detection of the signal of $Fc(MeOH)_2^{0/+1}$ (second current plateau) without any $Ru(NH_3)_6^{3+/2+}$ interference in this potential range. Notwithstanding, the third current plateau still suffers from the interference of $Fc(MeOH)_2^{0/+1}$, and the redox cycling current of I^- is superimposed by $Fc(MeOH)_2^{0/+1}$. In order to resolve this issue, the potential of the bottom electrode is next set at 0.4 V (Figure 2C). Here, for potentials above 0.26 V, only I^- can undergo redox cycling (third current plateau) and the signal is free from any interferences of both $Fc(MeOH)_2^{0/+1}$ and $Ru(NH_3)_6^{3+/2+}$. Note that at potentials above 0.26 V in Figure 2C, $Fc(MeOH)_2^{0/+1}$ is constantly oxidized at both electrodes, but it does not undergo redox cycling; this leads to a negligible current contribution (resulting to a deviation of 0.16%) compared to the amplified redox cycling current.

Using eq 5 and the constants in Table 1, the expected limiting currents are estimated to be 11 nA, 9 nA, and 30 nA for $Ru(NH_3)_6^{3+/2+}$, $Fc(MeOH)_2^{0/+1}$, and I^-, respectively, in good agreement with those obtained from experimental measurements (see Figure 2). The 30 nA oxidation current obtained for I^- (also presented in Figure 2C) indicates that this process is overall a one-electron transfer reaction in agreement with previous reports.[43−45] The hysteresis observed during the oxidation of iodide is caused by a pronounced desorption of iodide ions from the electrode surface during the forward scan and subsequent adsorption after the potential reversal.[46]

Differential Cyclic Voltammetry of Redox Species in the Nanogap Sensor. We employ the method of differential cyclic voltammetry[37] to directly visualize the separate sensing of all species in a single potential sweep. Here, the potentials of

DOI: 10.1021/acssensors.6b00556
ACS Sens. 2016, 1, 1439−1444

both electrodes are simultaneously swept with a constant offset. We define various potential windows of 10 mV, 25 mV, 50 mV, and 100 mV between the two working electrodes in the same mixture solution of 0.33 mM $Fc(MeOH)_2$, 0.33 mM $Ru(NH_3)_6^{3+}$, and 0.33 mM I^- in 1 M aqueous KCl. Once these potential windows are defined, a clear peak current is obtained for each redox species. The peak potential for each species corresponds to its redox potential.

Figure 3 shows the redox cycling currents obtained as a function of the mean potential between the top and bottom

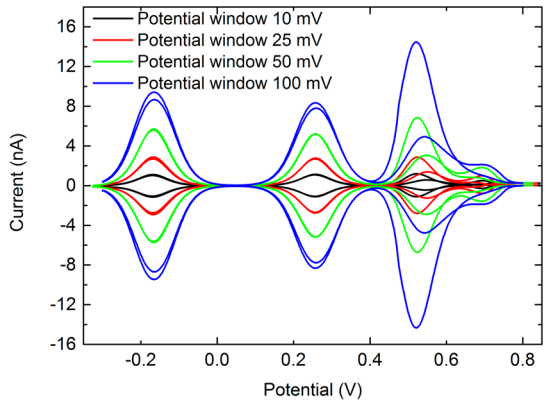

Figure 3. Differential cycling voltammetry in the nanogap sensor. The top and bottom electrodes are swept (vs Ag/AgCl) at a scan rate of 10 mV s^{-1} with a constant potential difference ranging from 10 mV to 100 mV. The limiting currents are shown as a function of mean potential between the two electrodes.

electrodes and a clear separation of all species. Due to the simultaneous sweep of both electrodes, the resulting currents have a differential nature. The peak currents at the half-wave potential of each species correspond to $\Delta I/\Delta E$ as well as to the species' concentration. As shown in Figure 3, a narrower potential window leads to a lower current but a better separation of species. For example, for a potential window of 10 mV, a peak current of 1.12 nA is obtained for $Fc(MeOH)_2^{0/+1}$ species, while for a 100 mV potential window, the current peaks at 7.8 nA. However, the full width at half-maximum (fwhm) increases from 92 mV for a 10 mV potential window to 125 mV for a 100 mV potential window. Therefore, a wider potential window limits how well the redox species are separated; the baseline distance between $Fc(MeOH)_2^{0/+1}$ peak and adjacent peaks is decreased by applying a wider potential window. The widest potential window that can be applied depends on the difference in the redox potentials of species. For example, the largest potential window for separate detection of $Fc(MeOH)_2^{0/+1}$ and I^- is 280 mV corresponding to $E_{h,I^-} - E_{h,Fc(MeOH)_2}$ = 280 mV (more details are presented in Figure S2 in the Supporting Information).

Chronoamperometric Detection of Redox Species in the Nanogap Sensor. In the two voltammetry schemes described above, the discriminatory power of specific electrode biases for both electrodes is shown in a direct way. However, the separate detection of analytes plays out its full advantage in chronoamperometric sensing with fixed potentials, in which redox waves of potential interfering species are not visible. We employed chronoamperometry in the nanogap sensor. Here, the device is filled with a mixture of 0.4 mM KI and 0.6 mM $Fc(MeOH)_2$ in 1 M KCl solution. A constant potential of 0.4 V vs Ag/AgCl is applied to the top electrode while the potential of the bottom electrode is stepped between 0.1 and 0.4 V and then between 0.4 and 0.7 V (see Figure 4).

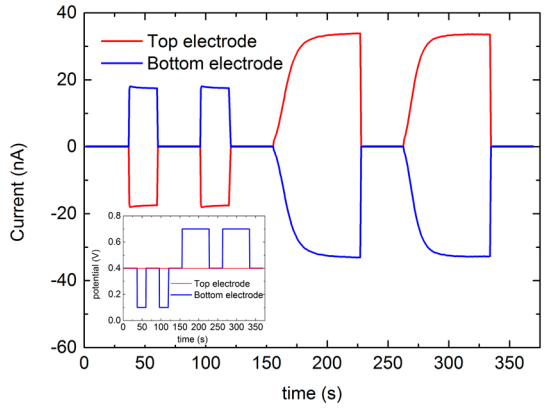

Figure 4. Chronoamperometry results obtained for a mixture of 0.6 mM $Fc(MeOH)_2$ and 0.4 mM KI in 1 M KCl solution. The inset shows the applied potentials as a function of time. The top electrode is kept at constant potential of 0.4 V and the bottom electrode is stepped to 0.1, 0.4, or 0.7 V.

Once the potential of the bottom electrode is stepped to 0.1 V, $Fc(MeOH)_2$ undergoes redox cycling (first two steps) without any interference from I^-. Here, $Fc(MeOH)_2$ is constantly oxidized at the top electrode and reduced at the bottom electrode. Similarly, when the bottom electrode potential is stepped to 0.7 V, I^- ions undergo redox cycling without any interference from $Fc(MeOH)_2^{0/+1}$. I^- is constantly oxidized at the bottom electrode and reduced at the top electrode. At the same time, $Fc(MeOH)_2^{0/+1}$ is constantly oxidized at both top and bottom electrodes, but since they cannot undergo redox cycling, their contribution to the current for I^- is negligible (resulting in a deviation of 0.3%). These results are in good agreement with those obtained from cyclic voltammetry. The long transient time for I^- is due to the dynamic adsorption at the Pt electrode surfaces.[46−48]

Numerical Analysis. Figure 5 shows the comparison of cyclic voltammetry as well as differential cyclic voltammetry of 0.33 mM $Ru(NH_3)_6^{3+}$, 0.33 mM $Fc(MeOH)_2$, and 0.33 mM I^- in 1 M KCl for experimental measurements and finite element simulation results. Figure 5 A presents the simulated data and its comparison with experimental cyclic voltammograms; here, the top electrode potential is swept between −0.33 and 0.8 V (vs Ag/AgCl) and the bottom electrode potential is kept at −0.3 V. Figure 5 B presents differential cyclic voltammograms for the potential window of 100 mV for both experimental and modeled results. As depicted, simulated data match well with experimental data. However, a hysteresis is observed experimentally for the oxidation and reduction of I^- due to pronounced adsorption of I^-,[46] which has not been considered in the simulations.

CONCLUSION

We proposed a novel strategy for the separate detection of redox active species in nanogap sensors and implemented it in three ways: first, by tuning the electrode potentials only desired species undergo redox cycling; hence, the obtained current is free of any interferences (shown for both cyclic voltammetry and chronoamperometric measurements). Second, by defining a potential window between the two electrodes and

DOI: 10.1021/acssensors.6b00556
ACS Sens. 2016, 1, 1439−1444

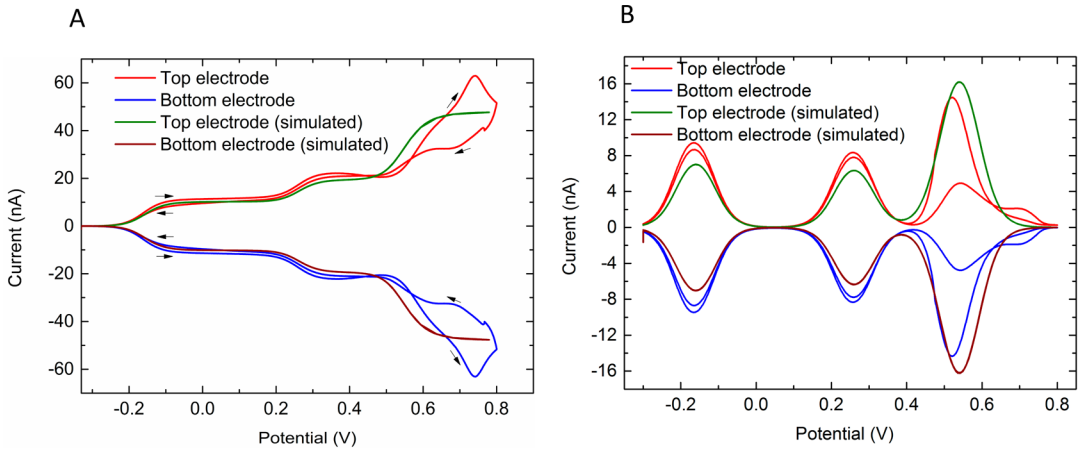

Figure 5. (A) Comparison of cyclic voltammograms (at a scan rate of 10 mV s^{-1}) of a mixture of 0.33 mM $Ru(NH_3)_6^{3+}$, 0.33 mM $Fc(MeOH)_2$, and 0.33 mM I^- in 1 M KCl (see also Figure 2A) with those numerical results. Arrows indicate the scan direction. (B) Comparison of experimental and simulated differential cyclic voltammetry (at a scan rate of 10 mV s^{-1}) of a potential window of 100 mV (see also Figure 3).

simultaneously sweeping them, each species can individually undergo redox cycling. Third, by chronoamperometry specific concentrations can be monitored without interference by using a matching potential window. A good agreement was obtained between the experimental and simulation results. The techniques introduced in this study may lead to new ways for the selective detection of redox species in nanogap devices.

■ ASSOCIATED CONTENT

Supporting Information

The Supporting Information is available free of charge on the ACS Publications website at DOI: 10.1021/acssensors.6b00556.

Cyclic voltammetry (PDF)

■ AUTHOR INFORMATION

Corresponding Author

*E-mail: l.rassaei@tudelft.nl.

Notes

The authors declare no competing financial interest.

■ REFERENCES

(1) Akbar, S.; Anwar, A.; Kanwal, Q. Electrochemical determination of folic acid: A short review. *Anal. Biochem.* **2016**, *510*, 98−105.

(2) Rahi, A.; Karimian, K.; Heli, H. Nanostructured materials in electroanalysis of pharmaceuticals. *Anal. Biochem.* **2016**, *497*, 39−47.

(3) Er, E.; Çelikkan, H.; Erk, N. Highly sensitive and selective electrochemical sensor based on high-quality graphene/nafion nanocomposite for voltammetric determination of nebivolol. *Sens. Actuators, B* **2016**, *224*, 170−177.

(4) Chikkaveeraiah, B. V.; Bhirde, A. A.; Morgan, N. Y.; Eden, H. S.; Chen, X. Electrochemical immunosensors for detection of cancer protein biomarkers. *ACS Nano* **2012**, *6* (8), 6546−6561.

(5) Li, H.; He, J.; Li, S.; Turner, A. P. Electrochemical immunosensor with N-doped graphene-modified electrode for label-free detection of the breast cancer biomarker CA 15−3. *Biosens. Bioelectron.* **2013**, *43*, 25−29.

(6) Rassaei, L.; Olthuis, W.; Tsujimura, S.; Sudhölter, E. J.; van den Berg, A. Lactate biosensors: current status and outlook. *Anal. Bioanal. Chem.* **2014**, *406* (1), 123−137.

(7) Fojta, M.; Daňhel, A.; Havran, L.; Vyskočil, V. Recent progress in electrochemical sensors and assays for DNA damage and repair. *TrAC, Trends Anal. Chem.* **2016**, *79*, 160−167.

(8) Paleček, E.; Tkáč, J.; Bartošík, M.; Bertók, T. s.; Ostatná, V.; Paleček, J. Electrochemistry of nonconjugated proteins and glycoproteins. Toward sensors for biomedicine and glycomics. *Chem. Rev.* **2015**, *115* (5), 2045−2108.

(9) Kumar Jena, B.; Retna Raj, C. Gold nanoelectrode ensembles for the simultaneous electrochemical detection of ultratrace arsenic, mercury, and copper. *Anal. Chem.* **2008**, *80* (13), 4836−4844.

(10) Rassaei, L.; Marken, F.; Sillanpää, M.; Amiri, M.; Cirtiu, C. M.; Sillanpää, M. Nanoparticles in electrochemical sensors for environmental monitoring. *TrAC, Trends Anal. Chem.* **2011**, *30* (11), 1704−1715.

(11) Dutta, G.; Park, S.; Singh, A.; Seo, J.; Kim, S.; Yang, H. Low-Interference Washing-Free Electrochemical Immunosensor Using Glycerol-3-phosphate Dehydrogenase as an Enzyme Label. *Anal. Chem.* **2015**, *87* (7), 3574−3578.

(12) Liu, X.; Zhang, M.; Xiao, T.; Hao, J.; Li, R.; Mao, L. Protein Pretreatment of Microelectrodes Enables in Vivo Electrochemical Measurements with Easy Precalibration and Interference-Free from Proteins. *Anal. Chem.* **2016**, *88* (14), 7238−7244.

(13) Alwarappan, S.; Liu, G.; Li, C.-Z. Simultaneous detection of dopamine, ascorbic acid, and uric acid at electrochemically pretreated carbon nanotube biosensors. *Nanomedicine* **2010**, *6* (1), 52−57.

(14) Wu, J.; Suls, J.; Sansen, W. Amperometric determination of ascorbic acid on screen-printing ruthenium dioxide electrode. *Electrochem. Commun.* **2000**, *2* (2), 90−93.

(15) Raicopol, M. D.; Andronescu, C.; Atasiei, R.; Hanganu, A.; Vasile, E.; Brezoiu, A. M.; Pilan, L. Organic layers via aryl diazonium electrochemistry: towards modifying platinum electrodes for interference free glucose biosensors. *Electrochim. Acta* **2016**, *206*, 226−237.

(16) Retna Raj, C.; Ohsaka, T. Voltammetric detection of uric acid in the presence of ascorbic acid at a gold electrode modified with a self-assembled monolayer of heteroaromatic thiol. *J. Electroanal. Chem.* **2003**, *540*, 69−77.

(17) Li, Y.; Zhang, L.; Liu, J.; Zhou, S.-F.; Al-Ghanim, K. A.; Mahboob, S.; Ye, B.-C.; Zhang, X. A novel sensitive and selective electrochemical sensor based on molecularly imprinted polymer on a nanoporous gold leaf modified electrode for warfarin sodium determination. *RSC Adv.* **2016**, *6* (49), 43724−43731.

(18) Li, Y.; Song, H.; Zhang, L.; Zuo, P.; Ye, B.-c.; Yao, J.; Chen, W. Supportless electrochemical sensor based on molecularly imprinted polymer modified nanoporous microrod for determination of dopamine at trace level. *Biosens. Bioelectron.* **2016**, *78*, 308−314.

(19) Sun, C.-L.; Lee, H.-H.; Yang, J.-M.; Wu, C.-C. The simultaneous electrochemical detection of ascorbic acid, dopamine, and uric acid using graphene/size-selected Pt nanocomposites. *Biosens. Bioelectron.* **2011**, *26* (8), 3450−3455.

DOI: 10.1021/acssensors.6b00556
ACS Sens. 2016, 1, 1439−1444

(20) Thiagarajan, S.; Chen, S.-M. Preparation and characterization of PtAu hybrid film modified electrodes and their use in simultaneous determination of dopamine, ascorbic acid and uric acid. *Talanta* **2007**, *74* (2), 212−222.
(21) Idris, A. O.; Mafa, J. P.; Mabuba, N.; Arotiba, O. A. Dealing with interference challenge in the electrochemical detection of As(III) —A complexometric masking approach. *Electrochem. Commun.* **2016**, *64*, 18−20.
(22) Yin, T.; Wei, W.; Zeng, J. Selective detection of dopamine in the presence of ascorbic acid by use of glassy-carbon electrodes modified with both polyaniline film and multi-walled carbon nanotubes with incorporated β-cyclodextrin. *Anal. Bioanal. Chem.* **2006**, *386* (7−8), 2087−2094.
(23) Sadak, O.; Sundramoorthy, A. K.; Gunasekaran, S. Highly selective colorimetric and electrochemical sensing of iron (III) using Nile red functionalized graphene film. *Biosens. Bioelectron.* **2016**; DOI: 10.1016/j.bios.2016.04.073
(24) Kanno, Y.; Ino, K.; Shiku, H.; Matsue, T. A local redox cycling-based electrochemical chip device with nanocavities for multi-electrochemical evaluation of embryoid bodies. *Lab Chip* **2015**, *15* (23), 4404−4414.
(25) Barnes, E. O.; Lewis, G. E.; Dale, S. E.; Marken, F.; Compton, R. G. Generator-collector double electrode systems: A review. *Analyst* **2012**, *137* (5), 1068−1081.
(26) Niwa, O.; Morita, M.; Tabei, H. Electrochemical behavior of reversible redox species at interdigitated array electrodes with different geometries: consideration of redox cycling and collection efficiency. *Anal. Chem.* **1990**, *62* (5), 447−452.
(27) Hayashi, K.; Takahashi, J.-i.; Horiuchi, T.; Iwasaki, Y.; Haga, T. Development of nanoscale interdigitated array electrode as electrochemical sensor platform for highly sensitive detection of biomolecules. *J. Electrochem. Soc.* **2008**, *155* (9), J240−J243.
(28) Samarao, A. K.; Rust, M. J.; Ahn, C. H. In *Rapid fabrication of a nano interdigitated array electrode and its amperometric characterization as an electrochemical sensor*; Sensors, 2007 IEEE; IEEE, 2007; pp 644−647.
(29) Wolfrum, B.; Zevenbergen, M.; Lemay, S. Nanofluidic redox cycling amplification for the selective detection of catechol. *Anal. Chem.* **2008**, *80* (4), 972−977.
(30) Zevenbergen, M. A.; Wolfrum, B. L.; Goluch, E. D.; Singh, P. S.; Lemay, S. G. Fast electron-transfer kinetics probed in nanofluidic channels. *J. Am. Chem. Soc.* **2009**, *131* (32), 11471−11477.
(31) Rassaei, L.; Mathwig, K.; Kang, S.; Heering, H. A.; Lemay, S. G. Integrated biodetection in a nanofluidic device. *ACS Nano* **2014**, *8* (8), 8278−8284.
(32) Hasnat, M. A.; Gross, A. J.; Dale, S. E.; Barnes, E. O.; Compton, R. G.; Marken, F. A dual-plate ITO−ITO generator−collector microtrench sensor: surface activation, spatial separation and suppression of irreversible oxygen and ascorbate interference. *Analyst* **2014**, *139* (3), 569−575.
(33) Goluch, E. D.; Wolfrum, B.; Singh, P. S.; Zevenbergen, M. A.; Lemay, S. G. Redox cycling in nanofluidic channels using interdigitated electrodes. *Anal. Bioanal. Chem.* **2009**, *394* (2), 447−456.
(34) Martin, R. S.; Gawron, A. J.; Lunte, S. M.; Henry, C. S. Dual-electrode electrochemical detection for poly (dimethylsiloxane)-fabricated capillary electrophoresis microchips. *Anal. Chem.* **2000**, *72* (14), 3196−3202.
(35) Kätelhön, E.; Hofmann, B.; Lemay, S. G.; Zevenbergen, M. A.; Offenhäusser, A.; Wolfrum, B. Nanocavity redox cycling sensors for the detection of dopamine fluctuations in microfluidic gradients. *Anal. Chem.* **2010**, *82* (20), 8502−8509.
(36) van Megen, M.; Odijk, M.; Wiedemair, J.; Olthuis, W.; van den Berg, A. Differential cyclic voltammetry for selective and amplified detection. *J. Electroanal. Chem.* **2012**, *681*, 6−10.
(37) Odijk, M.; Wiedemair, J.; van Megen, M.; Olthuis, W.; van den Berg, A. In *Differential cyclic voltammetry-a novel technique for selective and simultaneous detection using redox cyling based sensors*; Sensors, 2010 IEEE; IEEE, 2010; pp 918−922.
(38) Zafarani, H. R.; Mathwig, K.; Sudhölter, E. J. R.; Rassaei, L. Electrochemical redox cycling in a new nanogap sensor: Design and simulation. *J. Electroanal. Chem.* **2016**, *760*, 42−47.
(39) Bard, A. J.; Faulkner, L. R. *Electrochemical methods: fundamentals and applications*; Wiley: New York, 1980; Vol. 2.
(40) Kolthoff, I.; Jordan, J. Voltammetry of iodine and iodide at rotated platinum wire electrodes. *J. Am. Chem. Soc.* **1953**, *75* (7), 1571−1575.
(41) Rassaei, L.; Mathwig, K.; Goluch, E. D.; Lemay, S. G. Hydrodynamic voltammetry with nanogap electrodes. *J. Phys. Chem. C* **2012**, *116* (20), 10913−10916.
(42) Ma, C.; Contento, N. M.; Gibson, L. R.; Bohn, P. W. Redox cycling in nanoscale-recessed ring-disk electrode arrays for enhanced electrochemical sensitivity. *ACS Nano* **2013**, *7* (6), 5483−5490.
(43) French, R. W.; Marken, F. Growth and characterisation of diffusion junctions between paired gold electrodes: diffusion effects in generator−collector mode. *J. Solid State Electrochem.* **2009**, *13* (4), 609−617.
(44) Marken, F.; Akkermans, R. P.; Compton, R. G. Voltammetry in the presence of ultrasound: the limit of acoustic streaming induced diffusion layer thinning and the effect of solvent viscosity. *J. Electroanal. Chem.* **1996**, *415* (1), 55−63.
(45) Tomčík, P.; Bustin, D. Voltammetric determination of iodide by use of an interdigitated microelectrode array. *Fresenius' J. Anal. Chem.* **2001**, *371* (4), 562−564.
(46) Mampallil, D.; Mathwig, K.; Kang, S.; Lemay, S. G. Reversible adsorption of outer-sphere redox molecules at Pt electrodes. *J. Phys. Chem. Lett.* **2014**, *5* (3), 636−640.
(47) Kang, S.; Mathwig, K.; Lemay, S. G. Response time of nanofluidic electrochemical sensors. *Lab Chip* **2012**, *12* (7), 1262−7.
(48) Mathwig, K.; Lemay, S. G. Mass transport in electrochemical nanogap sensors. *Electrochim. Acta* **2013**, *112*, 943−949.

DOI: 10.1021/acssensors.6b00556
ACS Sens. 2016, 1, 1439−1444

Supporting Information for:

Modulating selectivity in nanogap sensors

Hamid Reza Zafarani,[1] Klaus Mathwig,[2] Serge G. Lemay,[3] Ernst J. R. Sudhölter[1] and Liza Rassaei*[1]

[1] *Laboratory of Organic Materials and Interfaces, Department of Chemical Engineering, Delft University of Technology, Van der Maasweg 9, 2629 HZ Delft, The Netherlands*

[2] *Pharmaceutical Analysis, Groningen Research Institute of Pharmacy, University of Groningen, P.O. Box 196, 9700 AD, Groningen, The Netherlands*

[3] *MESA+ Institute for Nanotechnology, University of Twente, P.O. Box 217, 7500 AE Enschede, The Netherlands*

l.rassaei@tudelft.nl

Abstract

Herein, we present individual cyclic voltammograms of selected electroactive model compounds (I^- and $Ru(NH_3)_6^{3+}$) in the nanogap sensor (Figure S1). Figure S2 shows the simulated differential cyclic voltammograms in the nanogap with different potential windows. Here, we investigated the effect of the potential window on peak separation of redox species in differential cyclic voltammetry.

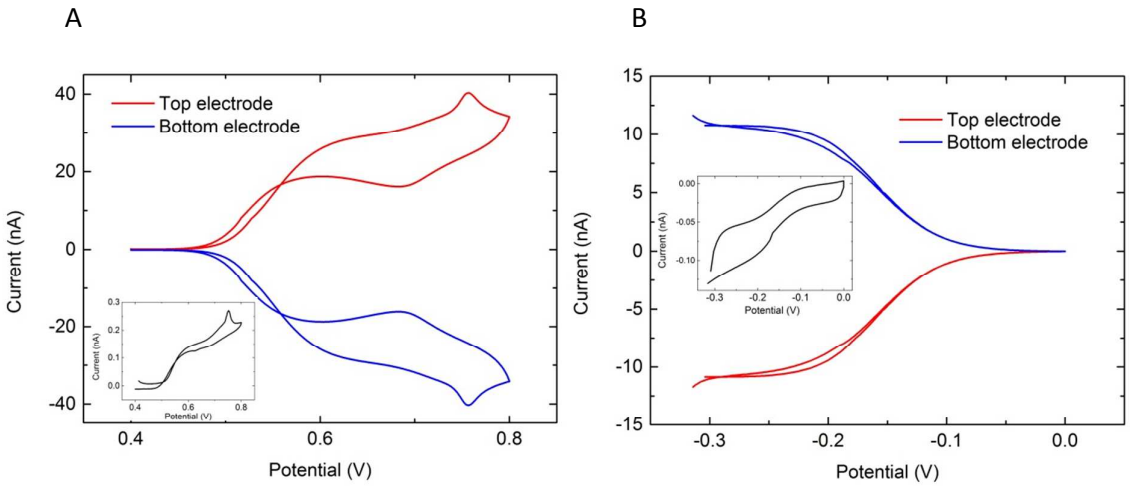

Figure S1. Cyclic voltammetry of individual species. (A) CV of 0.33 mM I^- in 1 M KCl solution. The top electrode was swept from 0.4 to 0.8 V (*vs.* Ag/AgCl) at a 10 mVs^{-1} scan rate while the bottom electrode was fixed at 0 V, (B) CV of 0. 33 mM $Ru(NH_3)_6^{3+}$ in 1 M KCl solution. Top electrode was swept from -0.33 to 0 V at a 10 mVs^{-1} scan rate while the bottom electrode was fixed at 0 V. The insets shows CVs in single mode. Here, only the top electrode was swept and the bottom electrode was kept floating.

As shown in Figure S1A, the characteristic peak current signal of I^- is presented in both cyclic voltammograms recorded in dual mode and in single mode.

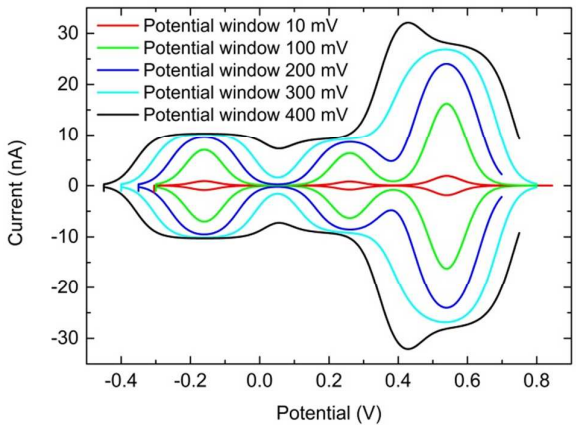

Figure S2. Modelled differential cycling voltammetry in the nanogap sensor. The top and bottom electrodes are swept with a constant potential difference ranging from 10 mV to 400 mV. The limiting currents are shown as a function of the mean potential between the two electrodes.

Figure S2 presents the simulated differential cyclic voltammograms in the nanogap sensor with different potential windows. Increasing the potential window between the two electrodes from 200 mV to 300 mV leads to the overlapping of the peak currents for $Fc(MeOH)_2$ and I^-; hence, selectivity is lost.